Microfluidic Generation of Gradient Hydrogels to Modulate Hematopoietic Stem Cell Culture Environment

*Bhushan P. Mahadik, Tobias D. Wheeler, Luke J. Skertich, Paul J. A. Kenis, and Brendan A. C. Harley**

The bone marrow provides spatially and temporally variable signals that impact the behavior of hematopoietic stem cells (HSCs). While multiple biomolecular signals and bone marrow cell populations have been proposed as key regulators of HSC fate, new tools are required to probe their importance and mechanisms of action. Here, a novel method based on a microfluidic mixing platform to create small volume, 3D hydrogel constructs containing overlapping patterns of cell and matrix constituents inspired by the HSC niche is described. This approach is used to generate hydrogels containing opposing gradients of fluorescent microspheres, MC3T3-E1 osteoblasts, primary murine hematopoietic stem and progenitor cells (HSPCs), and combinations thereof in a manner independent of hydrogel density and cell/particle size. Three different analytical methods are described to characterize local properties of these hydrogels at multiple scales: 1) whole construct fluorescent analysis; 2) multi-photon imaging of individual cells within the construct; 3) retrieval of discrete sub-regions from the hydrogel post-culture. The approach reported here allows the creation of stable gradients of cell and material cues within a single, optically translucent 3D biomaterial to enable a range of investigations regarding how microenvironmental signals impact cell fate.

1. Introduction

Hematopoiesis is a physiological process where the body's full complement of blood and immune cells are generated from a small number of hematopoietic stem cells (HSCs).[1–3] HSCs are primarily found in the bone marrow, a complex, 3D microenvironment consisting of cells, the extracellular matrix (ECM), as well as ECM-bound and soluble biomolecules.[2] This niche is believed to provide signals that dynamically influence HSC fate decisions, notably quiescence, self-renewal, and differentiation.[4] HSCs use a complex network for sensing, communication, and regulation that is likely hierarchical and integrates multiple microenvironmental inputs. However, relatively little is known about how HSCs assimilate and respond to multiple extrinsic cues from its microenvironment.

The rarity of HSCs within the bone marrow[2] challenges direct identification of key niche constituents and underlying mechanisms of action. Previous ex vivo HSC studies have highlighted increasingly sophisticated approaches to probe the influence of cell–cell interactions and paracrine-mediated signaling on HSC fate. HSCs cultured in conditioned media or co-cultured with endothelial cells and osteoblasts exhibit altered fate decisions.[5–7] Culture platforms have also recently been described to investigate the impact of combinations of growth factors.[8] While media supplementation and Transwell membrane experiments provide the capacity to study paracrine signaling in a limited manner, they are not amenable to reproduce the 3D cellular, biophysical, and biochemical gradients that exist within the native bone marrow.

While functional bone marrow mimics may eventually require spatiotemporal control over the distribution of multiple niche constituents within a single biomaterial, they must also facilitate analysis of the resultant fate decisions at multiple scales (single cell through cell populations).[9] Gradient materials are particularly attractive for such a platform due to their ability to present a continuous series of microenvironments across a single construct as well as their potential to mimic anatomical gradients found within the native bone marrow.[10] A number of approaches have recently been described for generating biomaterials containing defined gradients. Microfluidic platforms, and more recently photolithography approaches, have long been used to create spatial gradients of tethered and soluble biomolecules on 2D substrates.[11–14] Resultant studies employing these gradients have been used to examine a wide range of cellular processes such as motility and polarity.[15–20] Polyacrylamide substrates containing gradients in elastic modulus have also recently been used to study the impact of stiffness gradients on mesenchymal stem cell behavior.[21] While time consuming, bioprinting techniques have been increasingly used to spatially pattern ECM proteins, growth factors, and/or cells on 2D substrates in order to impact stem cell differentiation and bioactivity.[22,23]

While a wide range of methods have been reported for creating stable gradient on 2D substrates, techniques have only more recently begun to be described for creating stable

B. P. Mahadik, Dr. T. D. Wheeler, L. J. Skertich, Prof. P. J. A. Kenis, Prof. B. A. C. Harley
Department of Chemical and Biomolecular Engineering
University of Illinois at Urbana-Champaign
110 Roger Adams Lab, 600 S. Mathews St,
Urbana, IL, 61801, USA
E-mail: bharley@illinois.edu

Prof. P. J. A. Kenis, Prof. B. A. C. Harley
Institute for Genomic Biology
University of Illinois at Urbana-Champaign
1206 West Gregory Drive, MC-195 Urbana, IL 61801, USA

DOI: 10.1002/adhm.201300263

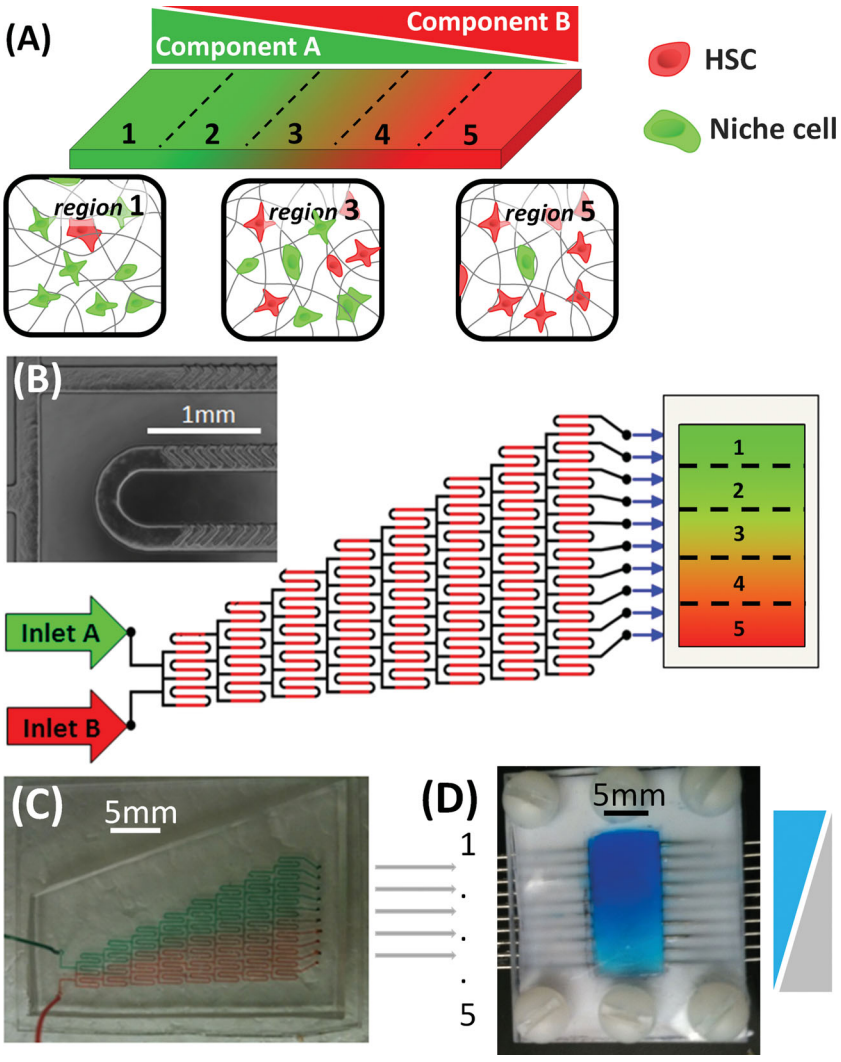

Figure 1. Concept and design of a microfluidic device to create hydrogels containing overlapping gradients of hydrogel or cellular components. A) Two-component opposing gradient hydrogel with overlapping patterns of matrix and cell content within discrete regions in the hydrogel. B) Schematic of microfluidic mixer that combines two inlet solutions (A,B) via a computer-controlled syringe pump. Geometric expansion leads to 10 outlets that enter a 180 µL Teflon mold. Inset: Microscopic image of mixing channel (200 µm wide × 100 µm deep) containing a herring-bone structure (50 µm) to indu ce chaotic advection. C) Macroscopic view of mixer containing colorized precursor suspensions. D) Macroscopic view of Teflon mold containing resultant counter gradient hydrogel A schematic depicting the concept of the gradient gels.

gradients within fully 3D biomaterials. Convective mixing of multiple hydrogel precursor solutions has been shown to allow the production of stable gradients within 3D hydrogels, though this method is most effective for creating gradients in narrow channels with extended aspect ratios (channel length significantly larger than width or depth).[24,25] Bioprinting techniques have been modified to create patterns of stem cells and biomolecules within fully 3D hydrogels in order to influence cell aggregation and migration.[26–32] Although promising, the time, complexity, and equipment required for creating these structures remains a concern. Microfluidic mixers have recently been described to create graded environments in fully 3D hydrogels, though typically these efforts have used microfluidic channels to impart a gradient in growth factor concentrations across an otherwise uniform hydrogel specimen.[33–35] Further, these approaches typically have not been used to generate gradients of cells within the final hydrogel; instead, cells are seeded on the surface of the hydrogels after they are formed. Such approaches preclude the generation of defined distribution patterns of cells within the final hydrogel structure.

The objective of this study was to develop a microfluidic mixing platform able to generate 3D hydrogels containing opposing gradients of multiple cell populations within the construct. Such a platform would leverage the relatively rapid speed for generating such gradients as well as the potential to modify mixing channel designs[36] to alter the width and geometry (linear, sinusoidal, exponential, sigmoidal) of the final gradient. We intend to use this platform as the basis for developing 3D culture environments that more closely replicate elements of the heterogeneous cell, matrix, and biomolecular environment within the bone marrow. Here, we adapted a conventional staggered herringbone microfluidic mixer[37] to generate a 3D hydrogel containing tunable, opposing gradients of cell and biomaterial properties from two hydrogel precursor suspensions (**Figure 1**). We show that stable multi-cell gradients can be created independent of cell size and hydrogel density without harming cell viability. Using this design, the relative ratio of the two cell types, their spacing, and the speed of diffusive transport through the hydrogel are all variables that can be spatially defined.

2. Results and Discussion

2.1. Hydrogels Containing Opposing Gradients of Fluorescent Microspheres

Opposing gradient hydrogels were first created using fluorescent microspheres (**Figure 2**) for a range of collagen hydrogel densities (1–2.5 mg mL^{-1}) that best reflect both typical working conditions for collagen hydrogels and the soft microenvironment within the bone marrow.[38–40] Slightly different optimized flow parameters were identified for each collagen density in order to create maximally reproducible counter-gradients (Table S1, Supporting Information). As expected, a higher flow rate (i.e., higher pressure) was required to achieve effective chaotic mixing for collagen suspensions of increased density. Hydrogels containing opposing linear gradients of fluorescent microspheres were used to compare three distinct analysis modalities with relevance for the resultant bone marrow

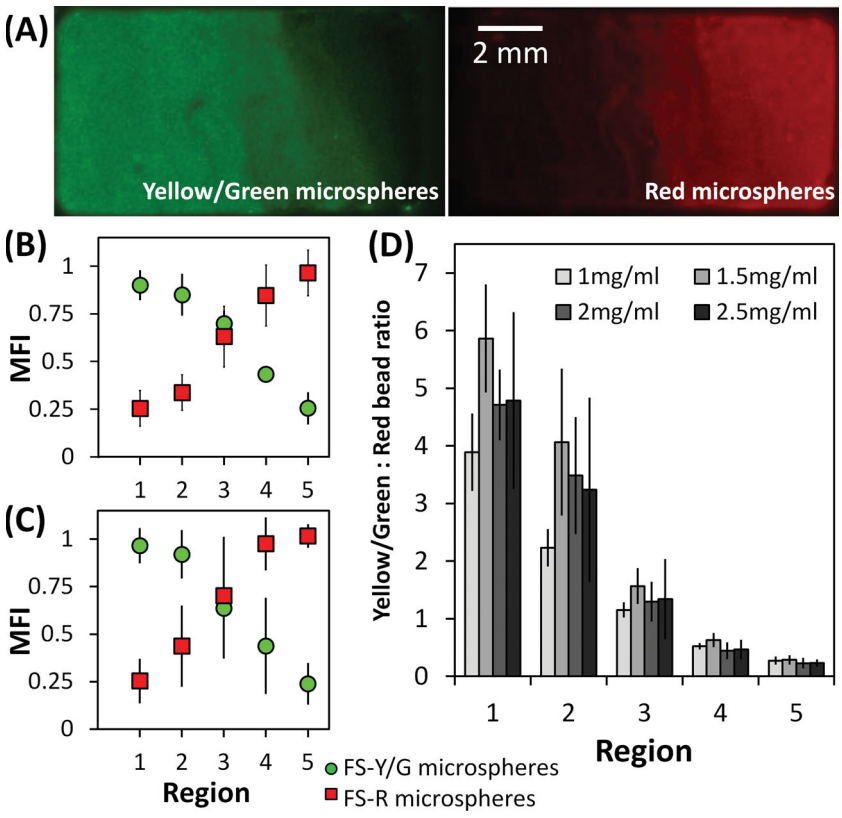

Figure 2. Collagen hydrogels containing overlapping gradients of multiple fluorescent microbeads. A) Spectrally separated images of the yellow/green fluorospheres (FS-Y/G) vs red fluorospheres (FS-R) populations within a single opposing gradient hydrogel. B) Normalized mean fluorescence intensity (MFI) for FS-Y/G vs FS-R populations along a 1.0 mg mL^{-1} gradient hydrogel. C) Normalized MFI for FS-Y/G vs FS-R populations along a 2.5 mg mL^{-1} gradient hydrogel. D) Ratio of FS-Y/G:FS-R within five standardized regions along the multi-gradient hydrogels (1.0, 1.5, 2.0, and 2.5 mg mL^{-1}).

mimics: 1) macroscopic analysis via fluorescent slide scanner; 2) microscopic analysis via confocal/two-photon imaging; 3) hydrogel segmentation and analysis via flow cytometry.

Results from all analyses are reported in terms of five standardized equally sized regions along the gradient (Figure 1A). Macroscopic analysis using a slide scanner confirmed the presence of opposing gradients of hydrogel precursor suspensions in the final hydrogel construct for a range of collagen densities (1–2.5 mg mL^{-1}). Figure 2A shows distinct gradients of yellow/green fluorescent microbeads (FS-Y/G) versus red fluorescent microbeads (FS-R) across a full 1.5 mg mL^{-1} collagen hydrogel. Figure 2B,C show mean fluorescence intensity (MFI) analysis confirming the presence of opposing linear gradients of microspheres for two hydrogel variants: 1.0 mg mL^{-1} (Figure 2B), 2.5 mg mL^{-1} (Figure 2C). Figure 2D depicts the ratio of the two microsphere populations across the five standardized analysis regions for all four hydrogel densities created. Critically, linear opposing gradients of microsphere populations were created for all tested hydrogel densities.

While a statistically significant ($p < 0.05$) change in FS-Y/G and FS-R MFI between each region was not always observed, the overall trend was statistically significant for all hydrogel densities. Slight non-uniformity in the resultant gradients can be noted across many gels. This can be attributed to speed of gelation of the collagen system, which relies on temperature induced gelation processes as well as the difficulty in maintaining a uniform flow across a large 8 mm mold width. Shrinking the size of the resultant multi-gradient hydrogel and using photocross-linkable chemistries are currently being pursued to create more stable opposing gradients. While previous literature has suggested that herringbone structures are not necessary to ensure uniform mixing,[11] the presence of heterogeneities (e.g., beads, cells) within our precursor suspensions required the presence of herringbone mixing structures to create linear gradients within the hydrogel (Figure S1, Supporting Information). Microbead-laden hydrogels created using an identical mixer geometry that lacked the herringbone structures contained microbead populations concentrated to either end of the construct, but not mixed across the construct, suggesting that herringbone structures are required to generate stable opposing gradients.

We subsequently used fluorescence activated cell sorting (FACS) analysis to validate the capacity to isolate distinct regions from within the hydrogel for post-culture analysis. The five standard regions along the gradient were isolated from the gradient hydrogel using a custom metal die inserted into the hydrogel, resuspended in PBS in order to break up the gels, and analyzed via flow cytometry in order to confirm the presence of opposing gradients of fluorescent microbeads (**Figure 3**) consistent to results obtained via the slide scanner (Figure 2). For a representative (1.5 mg mL^{-1}) hydrogel variant, region 1 contained an 85:15 FS-Y/G:FS-R ratio, region 3 contained a 46:54 FS-Y/G:FS-R ratio, and region 5 contained a 15:85 FS-Y/G:FS-R ratio. The Y/G:R ratio varied from 5.6:1 to 1:5.6, slightly different from the ratios obtained via the fluorescence slide scanner (≈4.5:1 to 1:4.5, Figure 2D). Such differences are likely due to detection efficiencies of each characterization method. However, overall these results demonstrate the potential to analyze either the hydrogel as a whole or distinct regions from within the hydrogel, a critical capacity for analyzing local versus global cell interactions across a gradient biomaterial.

2.2. Influence of Microfluidic Mixing Conditions on Cell Viability

Chaotic advective mixing has the potential to exert shear stresses on cells within the hydrogel suspension. While previous studies have indicated shear-mediated flow can be a negative regulator of cell viability,[41] HSCs natively mobilize into the peripheral blood stream and home back to the marrow, suggesting a capacity to withstand shear stresses associated

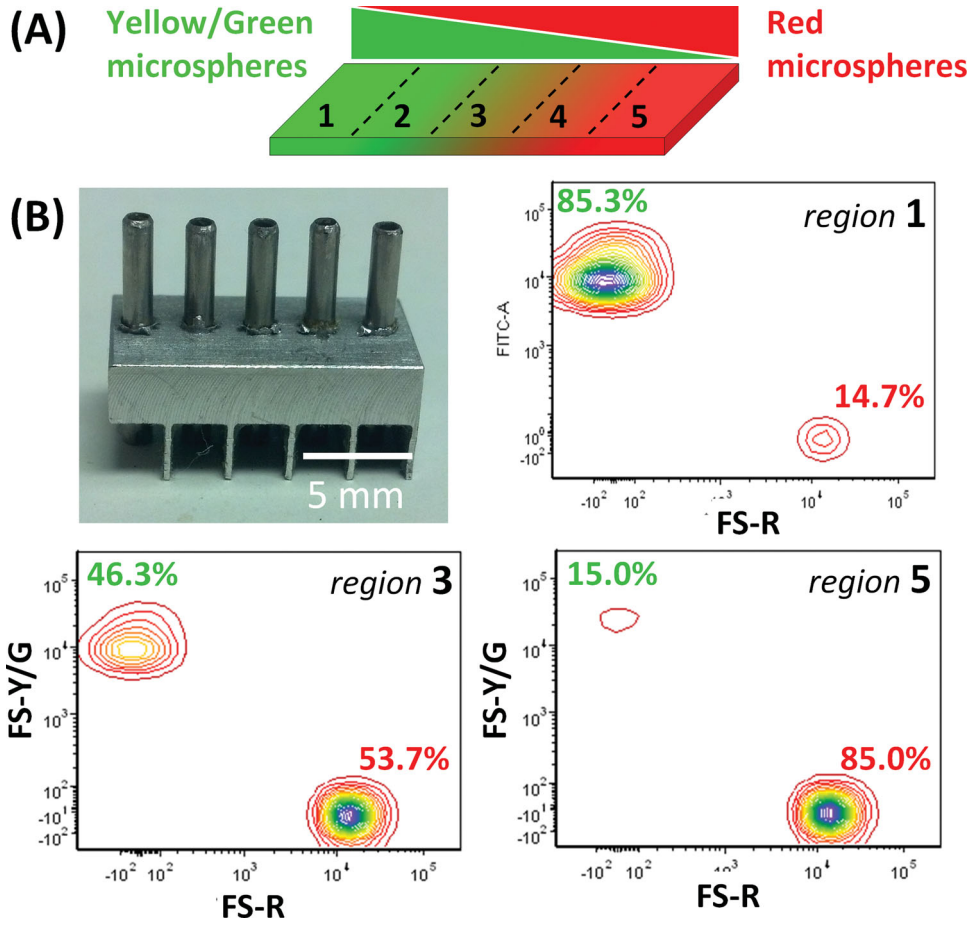

Figure 3. Isolating subregions from the gradient hydrogel for FACS analysis. A) Schematic of a counter-gradient hydrogel composed of yellow/green fluorospheres (FS-Y/G) vs red fluorospheres (FS-R). B) Metal die insert used to divide the hydrogel into five distinct hydrogel regions along the gradient. C) Characteristic FACS plots for hydrogel regions along the gradient with relative percentage of FS-Y/G (green) or FS-R (red) characteristic of MFI analysis results.

with blood flow.[42–44] To examine the impact of flow through the mixer on cell viability, 1 mg mL^{-1} collagen suspensions containing MC3T3-E1 or primary LSK cells were alternatively placed directly into a glass-bottom MatTek dish (control) or were passed through the microfluidic mixer (device) into the dish. Relative cell viability was assessed up to 3 d (**Figure 4**; Figure S2, Supporting Information). For both cell types, a high degree of relative viability was observed over the first 24 h of culture, the period of time during which the most significant effects of applied shear stress were expected.[45] While some statistically significant differences in viability were observed after 3 d in culture, viability remained high (>60%) throughout.

Notably, these results are consistent with previous observations involving a microfluidic device with channel dimensional and fluid flow rates smaller than those used here.[8] This prior work suggested that flow-induced cytotoxicity of HSPCs in microfluidic culture platforms is limited, in agreement with results reported here. While only examining flow-induced changes on cell viability here, ongoing experimental efforts are examining the role played by channel dimension, advective mixing conditions, hydrogel density, and flow rate on HSPC function (e.g., self-renewal vs proliferation). Such an approach would be critical for addressing the functional significance of applied shear stresses on HSPC fate or for investigating

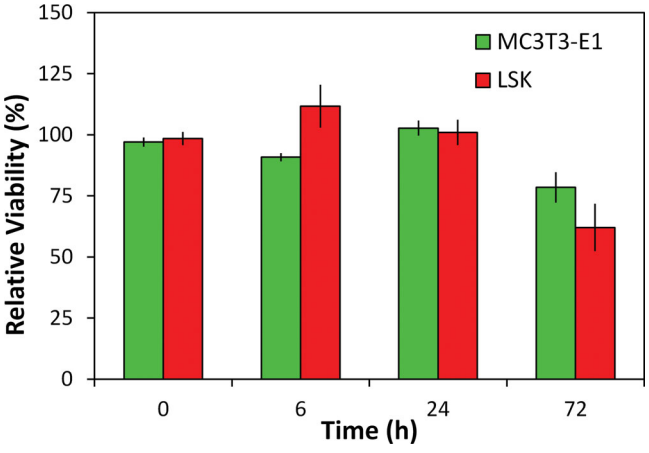

Figure 4. Relative viability of MC3T3 and LSK cells in 1 mg mL^{-1} collagen hydrogel after passing through the microfluidic mixer.

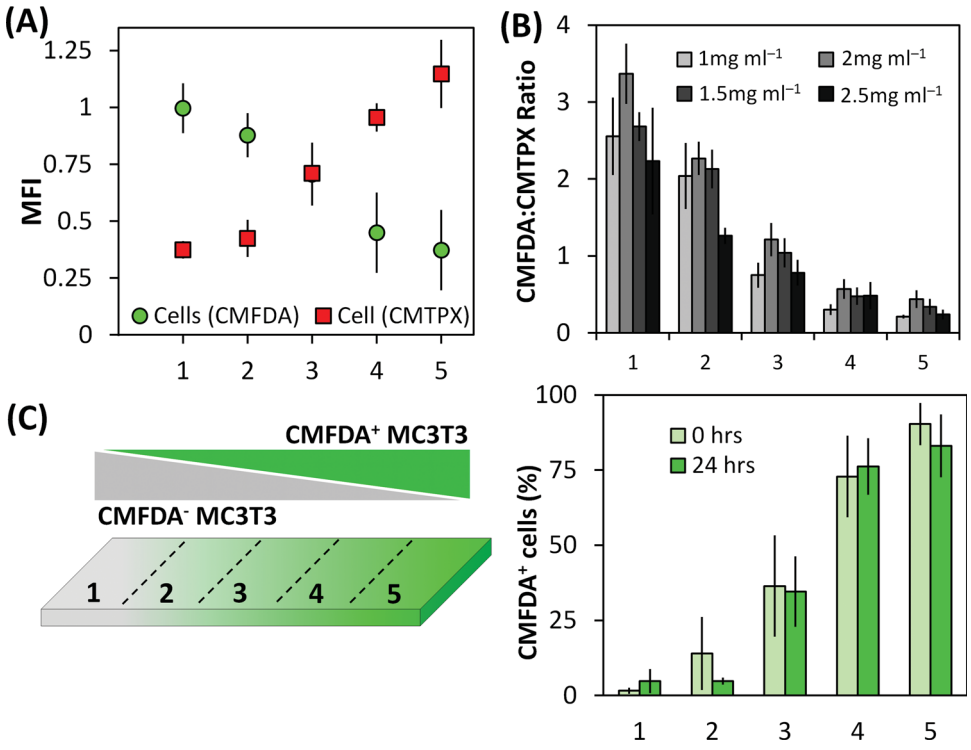

Figure 5. Collagen hydrogels containing overlapping gradients of multiple fluorescently tagged cell types. A) Normalized mean fluorescent intensity (MFI) for CMFDA vs CMTPX-labeled MC3T3 cells within five standardized regions along a 1 mg mL^{-1} collagen gradient hydrogel. B) Ratio of CMFDA:CMTPX labeled MC3T3 cells for all hydrogel densities (1.0, 1.5, 2.0, 2.5 mg mL^{-1}). C) FACS analysis of the fraction of CMFDA$^+$ MC3T3 cells (vs unlabeled MC3T3s) within each region of the hydrogel immediately after hydrogel formation (0 h) and after 24 h of culture.

mechanisms by which HSPCs sense shear stresses during mobilization from the bone marrow into the blood stream.

2.3. Hydrogels Containing Opposing Gradients in Cell Content

The ability to create opposing gradients of multiple cell populations within the hydrogel was demonstrated in a manner identical to that described for fluorescent microspheres. Opposing gradients of fluorescently tagged MC3T3s (with CMFDA-green dye and CMTPX-red dye) were observed via MFI analysis across all collagen densities (1–2.5 mg mL^{-1}; **Figure 5**). Figure 5A shows counter-gradients of MC3T3 cells for a representative hydrogel (1 mg mL^{-1}). Figure 5B depicts the CMFDA:CMTPX ratio within the five regions for all hydrogel variants. Similar to the microbead gradients, a statistically significant ($p < 0.05$) change in MFI was observed in the direction of the gradient across the hydrogel even though adjacent regional differences were not always statistically significant. Differences in MFI ratios between cell (3:1 to 1:3, Figure 5B) and microsphere (4.5:1 to 1:4.5, Figure 2D) laden hydrogels may be due to differences in chaotic mixing of ≈20 µm cells and 1 µm microbeads. Although this is an unavoidable occurrence in the presence of cells, modifications in microchannel dimensions could possibly alleviate these problems.

The stability of the cell gradients was subsequently assessed via FACS from hydrogels created using opposing gradients of unlabeled and CMFDA-labeled MC3T3s in 1.0 mg mL^{-1} collagen hydrogels (Figure 5C). The lowest hydrogel concentration was chosen as it was expected to present the least steric resistance to cell movement. The fraction of CMFDA$^+$ cells across the hydrogel was analyzed via FACS both immediately after hydrogel creation (0 h) and after 1 d in culture (24 h). Consistent gradients were observed (Figure 5C), suggesting the microfluidic device can be used to establish stable opposing gradients of cell content. Notably, a statistically significant ($p < 0.05$) increase in CMFDA$^+$ MC3T3s was observed across the gradient hydrogel at both 0 and 24 h, with no significant difference in CMFDA$^+$ fraction within any discrete region. While long-term remodeling is likely to disrupt these gradients, this current device will enable short-term analysis of cell–cell interactions. In addition to aiding the analysis of gradient stability, the ability to reproducibly isolate discrete regions from within the hydrogel is expected to play a particularly significant role in analyzing HSC fate decisions in future experiments where HSCs could be isolated from distinct regions of the hydrogel for not only FACS analysis, but also for further molecular biology techniques such as real-time polymerase chain reaction (RT-PCR) or signal transduction pathway analysis.

As an alternative, confocal microscopy was used to examine hydrogels containing opposing gradients of CMFDA$^+$ versus CMTPX$^+$ MC3T3s without having to disrupt the hydrogel culture. Our goal was to demonstrate the ability to use 3D imaging approaches to characterize local regions within the gradient hydrogel and do so in a manner conducive to continuous, live-cell monitoring of individual or small groups of cells within

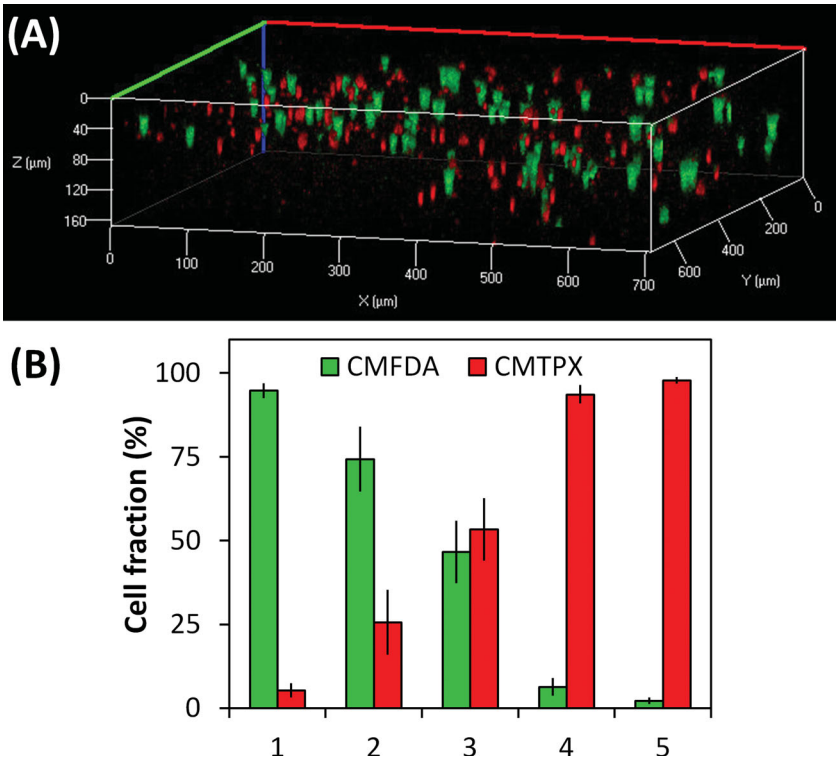

Figure 6. Confocal analysis of collagen hydrogels containing overlapping gradients of multiple fluorescently tagged cells. A) Confocal microscope image taken within subregion three along the gradient showing the relative density of CMFDA vs CMTPX labeled MC3T3 cells. B) Fraction of CMFDA vs CMTPX MC3T3 cells within the five regions along the gradient calculated from confocal images via manual cell counting.

the heterotypic hydrogel microenvironment. Qualitative assessment of image stacks acquired from each of the standardized hydrogel regions (**Figure 6**A, Region 3) suggests that confocal or multi-photon imaging could be used to describe the local cellular microenvironment. Subsequently, the total number of $CMFDA^+$ versus $CMTPX^+$ MC3T3s was manually counted within each image stack (Figure 6B). Linear opposing gradient were observed for all hydrogel densities (1–2.5 mg mL^{-1}). Taken together, these results suggest that local features within the hydrogel can be described via population level analysis of the entire construct (Figure 5A) or at the single-cell level via fluorescent microscopy (Figure 6B).

2.4. Diffusivity of the Hydrogel Matrix

To simulate paracrine-mediated intracellular signaling, we examined small-molecule diffusivity in monolithic collagen hydrogels (1–2.5 mg mL^{-1}) using fluorescein isothiocyanate (FITC)-conjugated dextran (40 kDa). Hydrogel diffusivity was high for all hydrogel densities: 150 ± 4 (1.0 mg mL^{-1}), 143 ± 10 (1.5 mg mL^{-1}), 137 ± 6 (2.0 mg mL^{-1}), and 153 ± 10 (2.5 mg mL^{-1}) $\mu m^2\ s^{-1}$. While a direct correlation between increasing collagen hydrogel density and mechanical integrity exists,[38] small-molecule diffusivity was not significantly affected for the range of collagen hydrogels explored here. Although the cells within the hydrogel could act as impermeable objects that hinder biomolecule diffusion,[46] cell densities (up to 5E6 cells mL^{-1}) were chosen such that they composed less than 7% of the total hydrogel volume. However, we anticipate that the magnitude of niche cell paracrine signals reaching an HSPC within the network to be a function of the local diffusivity of the matrix as well as the local density of niche cells. While such effects are the subject of ongoing investigations, the platform described in this study enables study of the impact of paracrine-mediated niche cell signaling on HSC fate through control over both matrix diffusivity and niche cell density.

2.6. Heterotypic Bone Marrow Microenvironment Mimics

The microfluidic mixing platform was then used to generate preliminary heterotypic bone marrow culture environments. Here, opposing gradients of primary murine LSK (HSPCs) and MC3T3 osteoblasts were created in 1 mg mL^{-1} collagen hydrogels. While MC3T3 osteoblasts are not expected to be functional niche cells capable of influencing hematopoiesis, the objective of this effort was to demonstrate that opposing linear gradients could be created from multiple cell types of different sizes (MC3T3 osteoblasts, ≈20 μm; LSKs, ≈5 μm) as the precursor to ongoing work using primary niche cells isolated from the bone marrow. Opposing gradients of LSKs and osteoblasts were quantified via whole construct fluorescence (**Figure 7**B,C). Notably, similar opposing gradients of MC3T3s and LSKs (2:1 to 1:2, Figure 7C) were observed as previously seen for opposing MC3T3 gradients in 1 mg mL^{-1} collagen (Figure 5A). Multiphoton microscopy was used to image individual LSKs and Lin^+ (GFP^+) bone marrow cells mixed together in a single hydrogel construct. Here, spectral deconvolution methods were capable of discerning LSKs ($cKit^+Sca1^+$) from mature bone marrow (Lin^+) cells (Figure 7D). As expected for the LSKs,[47] Sca1 was expressed across the cell surface while cKit was expressed in punctuate regions. Features in the resulting gradient gel appear to be primarily set by in-channel mixing and fluid flow through the outlets, suggesting that cell precipitation or heterogeneities in the precursor suspensions within the syringes may be negligible due to the speed of hydrogel mixing, often faster than 1 min (Table S1, Supporting Information).

Taken together, these experiments demonstrate the capability to create heterotypic cell microenvironments and then to interrogate the resultant multi-cell aggregates at multiple scales. Notably, the multi-gradient hydrogel construct developed here offers the potential to perform HSC fate tracing assays within a model 3D microenvironment where the local cellular microenvironment can be systematically manipulated. Ongoing work is also exploiting this system to create gradients in the biophysical properties of the matrix and incorporating additional

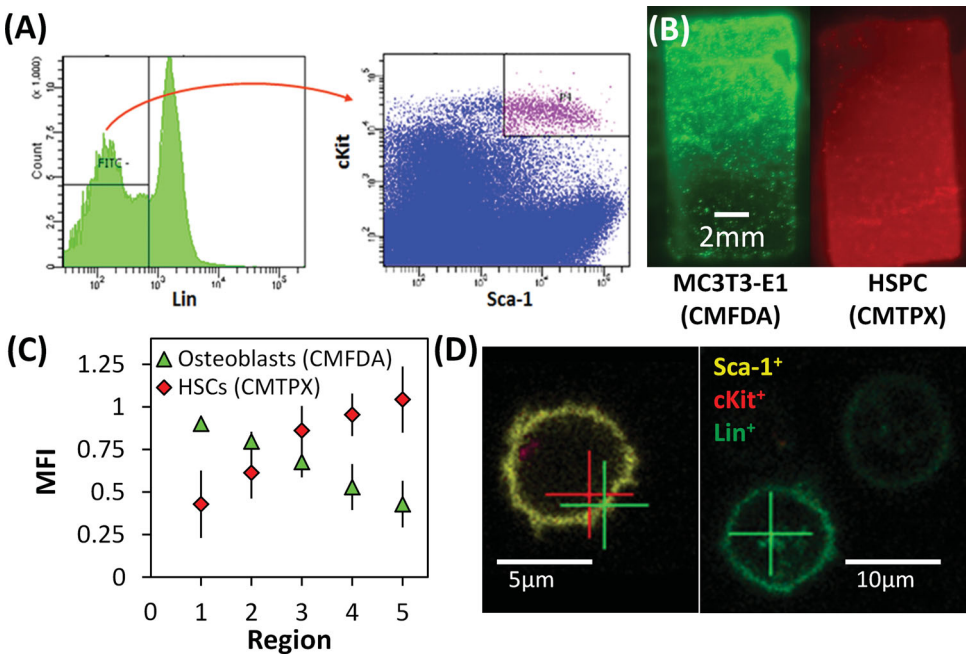

Figure 7. Incorporation of primary hematopoietic stem cells within the gradient hydrogel. A) FACS schematic of $Lin^{-}cKit^{+}Sca1^{+}$ cell isolation from the bone marrow of C57BL/6 mice. B) Spectrally separated images of the CMFDA-labeled MC3T3s vs CMPTX-labeled HSPCs within a single counter-gradient hydrogel (1 mg mL^{-1} collagen). C) Normalized mean fluorescent intensity (MFI) for $CMFDA^{+}$ MC3T3s vs $CMPTX^{+}$ HSPCs within 1 mg mL^{-1} collagen hydrogels. D) Non-destructive imaging of individual $cKit^{+}Sca1^{+}$ and Lin^{+} bone marrow cells within a 1 mg mL^{-1} collagen hydrogel via in situ two-photon microscopy.

microfluidic layers to provide local supplementation of cues such as growth factors to the hydrogel.[48] Efficient post-culture retrieval of local subregions of the hydrogel construct offers the potential to analyze region-specific HSC gene expression, signaling pathway analyses, and functional capacity (colony-forming unit, in vivo repopulation assays).[49,50] Future investigations leveraging this technology are anticipated to provide significant new information regarding how HSCs interact and respond to the diverse biophysical environment within the bone marrow.

3. Conclusions

We described an approach to reproducibly create heterotypic microenvironments containing HSCs and one or more putative niche cells in counter-gradient hydrogels. We have used multiple analytical approaches to validate the multi-gradient hydrogels at many scales (single cell to whole construct). We also described a method to extract distinct sub-regions from the greater hydrogel matrix for analysis using conventional molecular biology approaches. We demonstrated fabrication and maintenance in culture of a series of hydrogels containing opposing gradients of fluorescent microspheres, cell populations of similar size, or dissimilar sizes. Preliminary cell culture assays with both a cell line (MC3T3s) and primary stem cell population (LSK) indicated that viability was not significantly affected by microfluidic patterning.

The eventual goal of this effort is to develop a versatile biomaterial platform able to create complex patterns of niche inspired signals in order to examine the impact of biophysical cues and niche cell paracrine signaling on HSC fate. In addition to helping generate significant new knowledge regarding how micro-environmental signals help shape HSC fate decisions, this system may also facilitate optimization of culture platforms for ex vivo expansion of clinically relevant hematopoietic cell populations as well as study of the etiology, expansion, and treatment of hematopoietic pathologies.

4. Experimental Section

Fabrication of the Microfluidic Mixer and Hydrogel Mold: The microfluidic device was fabricated using standard two layer photolithography procedures on a 4″ Si wafer (University Wafers, South Boston, MA).[51] The design of the microfluidic diffusive mixer contains channels with a 200 μm (wide) × 100 μm (tall) cross-section with 50 μm high staggered herringbone features. These herringbone features induce chaotic advection in the channel that further facilitates mixing of cells.[37] The design for the device was created in Freehand MXTM (Macromedia Inc.) and printed on high-resolution transparencies (5080 dpi, University of Illinois at Urbana-Champaign Printing Services). A positive relief structure of the microchannel design was obtained by covering a silicon wafer with a 100-μm layer of SU8–2050 negative photoresist (MicroChem Corporation, Newton, MA) via spin-coating, baking (65 °C for 5 min, 95 °C for 15 min), and subsequently using UV exposure (OAI 1500, 220 mJ cm^{-2}) through the photomask that defines the channel geometry. A second 50 μm layer of photoresist was spin-coated onto the microchannel geometry, followed by baking and UV exposure (180 mJ cm^{-2}) with a herringbone photomask. The resulting two-layer photoresist structure was baked (65 °C for 1 min, 95 °C for 6 min) and then developed using propylene glycol monomethyl ether acetate (PGMEA). The remaining positive relief structure was then washed away with acetone and isopropyl alcohol. A monolayer of tridecafluoro-1,1,2,2-

tetrahydrooctyl trichlorosilane (Gelest, Morrisville, PA) was deposited onto the silicon master prior to replica molding to prevent covalent adhesion of polydimethylsiloxane (PDMS) on the photoresist and the silicon surfaces. PDMS devices were then created from this master by curing a 10:1 mixture of monomer:cross-linking agent (RTV 615 Part A/B, General Electric, Waterford, NY) on the wafer at 65 °C for 1 h. After peeling the PDMS mold off the wafer, access ports were punched using a 20-gauge needle. The mold was first cleaned with tape (Scotch TM 3M), and sealed to a plasma treated (Harrick Scientific Corp., PDC001) 3″ × 2″ glass slide (Fischer Scientific 12–550-A3), followed by annealing at 65 °C for 1 h.

The microfluidic mixer was designed to combine two hydrogel inputs (Component A, Component B) to create 10 output streams (Figure 1A), each with a defined ratio of the 2 inlet components. A Teflon mold with inner dimensions of 15 mm × 8 mm × 1.5 mm (≈180 µL) was made with 10 stainless steel tubes (25 Gauge) attached to either side of the 15 mm length of the mold close to the top surface. The tubes were press-fit into holes punched at each outlet of the microfluidic mixer and into the Teflon frame to physically connect the microfluidic mixer and the mold. Tubes press-fit into the opposite side of the Teflon frame served as outlets for the displaced volume within the mold during gradient formation (Figure S3, Supporting Information). Glass coverslips were semi-permanently attached to the top and bottom of the mold via non-toxic, non-reactive high-vacuum grease (Dow Corning). The coverslips were placed to facilitate live-cell fluorescent imaging within the gradient construct as well as post-culture removal to facilitate access to discrete regions of the hydrogel.

MC3T3 and HSPC Cell Culture: MC3T3-E1 pre-osteoblasts (MC3T3, ATCC, Manassas VA, passage 20–30) were cultured in T25 flasks in complete alpha-MEM media (minimum essential medium (MEM) with alpha modification, 10% fetal bovine serum (FBS), 5% Penicillin-Streptomycin, 5% L-Glutamine). MC3T3s were cultured to confluence at which point they were washed in PBS and trypsinized; cells were then either re-suspended in culture for expansion or prepared for use in the microfluidic devices. Prior to use, cells were fluorescently tagged via CMFDA (green) or CMTPX (red) fluorescent dye (Invitrogen, Carlsbad CA) at a 1:1000 dilution in complete alpha-MEM media (15 min; 37 °C).[52]

Primary HSPCs were isolated from the bone marrow of the femur and tibia of female C57BL/6 mice (Jackson Labs; Ages 1–3 months). The bones were gently crushed with a mortar and pestle, washed with a solution of PBS + 2% FBS (PBS/FBS), and filtered with a 40-µm sterile filter to isolate whole bone marrow. All subsequent steps were performed in a PBS/FBS solution on ice. Red blood cells were lysed with ACK lysis buffer (Invitrogen, Carlsbad, CA). Cells were re-suspended in PBS with Fc receptor-blocking antibody to reduce non-specific antibody binding. HSPCs were identified as the $Lin^{-}Sca\text{-}1^{+}c\text{-}kit^{+}$ (LSK) fraction by incubating the remaining bone marrow cells with a cocktail of antibodies: PE-conjugated Sca-1 (1:100 dilution), APC-conjugated c-kit (1:100 dilution), and a 1:100 dilution of an FITC-conjugated Lineage (Lin) cocktail (CD5, B220, Mac-1, CD8a, Gr-1, Ter-119).[53–55] All antibodies were supplied by eBioscience (San Diego, CA). The LSK fraction was then sorted using a BD FACS Aria II flow cytometer (BD FACS Diva software) and collected in PBS/FBS on ice for immediate use. An average of 0.2% of total bone marrow cells sorted was identified as LSK, consistent with previously reported results.[53–55] All animal experiments were conducted with permission obtained from the University of Illinois Institutional Animal Care and Use Committee (IACUC), Protocol #09054, #12033.

Preparation of Collagen Hydrogel Solutions Containing Fluorescent Microbeads or Cells: Type I collagen (BD Biosciences, Bedford MA) was used as the hydrogel precursor suspension for all experiments. Collagen solutions with defined densities (1.0, 1.5, 2.0, 2.5 mg mL^{-1}) were prepared from the stock collagen solution of approximately 9 mg mL^{-1} (lot specific) by mixing the collagen stock solution with complete α-MEM media and HEPES solution (2.5% of final volume); final suspension pH was adjusted to 7.3–7.5 via 0.4 m NaOH.[56] Hydrogels containing 1-µm diameter yellow/green (FS-Y/G) (Excitation: 505/15 nm; Emission: 515/15 nm) or Red (FS-R) fluorescent microbeads (Excitation: 575/25; Emission: 610/25) (Invitrogen, Carlsbad, CA) were generated by vortexing 0.1% (v/v) beads with the collagen hydrogel solution. Similarly, MC3T3s or LSK HSPCs were mixed into the hydrogel at a concentration of 200 000–400 000 cells mL^{-1}. All steps were performed at 4 °C to minimize the potential for hydrogel gelation prior to mixing through the microfluidic mixer.

Generation of Multi-Gradient Hydrogels: To prevent air bubbles from being trapped inside the device, the entire device assembly (microfluidic mixer, mold, connecting conduits) was immersed in water under vacuum (40 Torr, 15 min). The two input solutions for the multi-gradient hydrogel were prepared in 1 mL syringes that were then placed on a computer-controlled syringe pump (Harvard Apparatus, model 33 twin syringe pump, Holliston MA). The flow rate of the hydrogel precursor suspensions as well as the flow duration was tuned in accordance with the hydrogel density (Table S1, Supporting Information) to facilitate chaotic mixing and the formation of a smooth gradient. After generating the gradient hydrogel, the Teflon mold was detached from the microfluidic mixer, submerged in culture media in a Petri dish, and maintained in an incubator for long-term culture. To maintain the reproducibility of the gradients, new microfluidic mixers were generated for each experiment.

Characterizing Hydrogel Gradients: A Typhoon 9400 fluorescence slide scanner (GE electronics) was used to assess the two-component gradients. Briefly, the projected fluorescence values through the thickness of the hydrogel and across the gradient were gathered, with the resultant composite image subdivided into 5 (standardized) equally sized regions (1–5) along the gradient. As controls, the monolithic precursor suspensions were placed onto glass slides and scanned in order to normalize the fluorescence levels quantified from the gradient hydrogel. The MFI of each region was subsequently determined for all acquired fluorescence channels using ImageJ in a manner previously described.[57] All fluorescence data were then normalized to the appropriate precursor gel solution fluorescence, yielding a normalized MFI for each region.

Hydrogels containing fluorescently labeled (CMFDA, CMTPX) cells were alternatively imaged using a Zeiss 710 multiphoton confocal microscope through the coverslip under the hydrogel mold. 3D image stacks (700 µm × 700 µm × 170 µm deep) were acquired in the plane of the hydrogel construct from each of the five regions along the gradient; the total number of CMFDA versus CMTPX labeled cells in each region was then quantified. The spectral deconvolution capabilities of the Zeiss 710 microscope were employed to image discrete LSK HSPCs via cKit (APC) and Sca1 (PE) flow cytometry antibodies as well as Lin^{+} (GFP^{+}) bone marrow cells within the collagen hydrogel.

To analyze discrete populations within each hydrogel region (1–5), we developed a metal die, which could be inserted into the hydrogel at any point during culture to mechanically separate the hydrogel into five equally sized regions along the gradient (Figure 3B). Each sub-region contained 20–30 µL of cell-hydrogel suspension that could be individually collected and analyzed. The microbead or cell-embedded constructs isolated from each hydrogel region were resuspended in PBS, filtered to remove the collagen and analyzed using a BD flow cytometer to quantify relative populations across the hydrogel gradient.

Quantifying Small Molecule Diffusion: Hydrogel diffusivity was measured via fluorescence recovery after photobleaching (FRAP) experiments using FITC-conjugated Dextran (40 kDa, Sigma Aldrich).[58–61] Here, a 1 mg mL^{-1} dextran solution in PBS was used to prepare the collagen precursor solutions of different densities (1–2.5 mg mL^{-1}), replacing the media suspension previously described. The collagen solution was spread over a MatTek dish and incubated overnight (37 °C, 5% CO_2). FRAP measurements were performed using the Zeiss 710 Multiphoton confocal microscope.[48] Briefly, a 80-µm diameter spot was bleached (laser intensity: 0.05 mW) at the center of the gel depth. The sample was bleached for 5 s and recovery for up to 15 min was traced via fluorescent imaging. The half time ($t_{1/2}$) of the recovery was calculated using the FRAP function available in the Zeiss software. The hydrogel diffusion coefficient (D) was subsequently calculated as:

$$D = \frac{w^2}{t_{1/2}} \quad (1)$$

where D is the diffusion coefficient, w is the photobleaching beam radius, and $t_{1/2}$ is the recovery half time.[58,62] A maximum of three spots were bleached per sample, spaced as far away from each other as possible to minimize after-effects of photobleaching on every subsequent measurement.

Cell Viability: Cell viability within the hydrogels was assessed using a live/dead cytotoxicity kit (Invitrogen) using Calcein AM (live) and ethidium homodimer (dead) as indicators.[63] Viability was quantified via fluorescence microcopy and ImageJ at 0, 6, 24, and 72 h of culture analysis.

Statistical Analysis: One-way analysis of variance (ANOVA) was performed on gradient measurements across different regions and collagen densities for the beads and cells followed by Tukey tests.[64] Significance was set at $p < 0.05$. At least $n = 4$ gradient gels were used for all analyses. In the figures, the error in each data point is reported as the standard error of the mean unless otherwise noted.

Supporting Information

Supporting Information is available from the Wiley Online Library or from the author.

Acknowledgements

The authors would like to acknowledge Barbara Pilas and Bernard Montez (Flow Cytometry Facility, UIUC) as well as Sunny Choi (ChBE, UIUC) for assistance with bone marrow cell isolation and flow cytometry, Dr. Mayandi Sivaguru (IGB, UIUC) for assistance with fluorescence imaging, Dr. Peter Yau and Dr. Brian Ismai (Protein Sciences Facility, UIUC) for assistant with fluorescence scanner analyses, and Dr. Amit Desai (ChBE, UIUC) regarding microfluidic mixer design. This work was partially supported by Grants #160673 and #189782 from the American Cancer Society, Illinois Division, Inc. This material is based upon work supported by the National Science Foundation under Grant No. 1254738. The authors are also grateful for additional funding provided by the Department of Chemical & Biomolecular Engineering and the Institute for Genomic Biology at the University of Illinois at Urbana-Champaign.

Received: June 28, 2013
Published online: August 29, 2013

[1] I. L. Weissman, *Cell* **2000**, *100*, 157.
[2] A. Wilson, A. Trumpp, *Nat. Rev. Immunol.* **2006**, *6*, 93.
[3] T. Yin, L. Li, *J. Clin. Invest.* **2006**, *116*, 1195.
[4] K. Tokoyoda, T. Egawa, T. Sugiyama, B. I. Choi, T. Nagasawa, *Immunity* **2004**, *20*, 707.
[5] J. Zhu, R. Garrett, Y. Jung, Y. Zhang, N. Kim, J. Wang, G. J. Joe, E. Hexner, Y. Choi, R. S. Taichman, S. G. Emerson, *Blood* **2007**, *109*, 3706.
[6] S. Harada, G. A. Rodan, *Nature* **2003**, *423*, 349.
[7] J. M. Butler, D. J. Nolan, E. L. Vertes, B. Varnum-Finney, H. Kobayashi, A. T. Hooper, M. Seandel, K. Shido, I. A. White, M. Kobayashi, L. Witte, C. May, C. Shawber, Y. Kimura, J. Kitajewski, Z. Rosenwaks, I. D. Bernstein, S. Rafii, *Cell Stem Cell* **2010**, *6*, 251.
[8] V. Lecault, M. Vaninsberghe, S. Sekulovic, D. J. Knapp, S. Wohrer, W. Bowden, F. Viel, T. McLaughlin, A. Jarandehei, M. Miller, D. Falconnet, A. K. White, D. G. Kent, M. R. Copley, F. Taghipour, C. J. Eaves, R. K. Humphries, J. M. Piret, C. L. Hansen, *Nat. Methods* **2011**, *8*, 581.
[9] C. R. Kothapalli, E. van Veen, S. de Valence, S. Chung, I. K. Zervantonakis, F. B. Gertler, R. D. Kamm, *Lab Chip* **2011**, *11*, 497.
[10] S.-Y. Park, P. Wolfram, K. Canty, B. A. Harley, C. Nombela Arrieta, G. Pivarnik, J. P. Manis, H. E. Beggs, L. E. Silberstein, *J. Immunol.* **2013**, *190*, 1094.
[11] N. L. Jeon, S. K. W. Dertinger, D. T. Chiu, I. S. Choi, A. D. Stroock, G. M. Whitesides, *Langmuir* **2000**, *16*, 8311.
[12] C. R. Toh, T. A. Fraterman, D. A. Walker, R. C. Bailey, *Langmuir* **2009**.
[13] D. Irimia, S. Y. Liu, W. G. Tharp, A. Samadani, M. Toner, M. C. Poznansky, *Lab Chip* **2006**, *6*, 191.
[14] I. Barkefors, S. Le Jan, L. Jakobsson, E. Hejll, G. Carlson, H. Johansson, J. Jarvius, J. W. Park, N. Li Jeon, J. Kreuger, *J. Biol. Chem.* **2008**, *283*, 13905.
[15] R. C. Gunawan, J. Silvestre, H. R. Gaskins, P. J. A. Kenis, D. E. Leckband, *Langmuir* **2006**, *22*, 4250.
[16] J. Silvestre, P. J. A. Kenis, D. E. Leckband, *Langmuir* **2009**, *25*, 10092.
[17] R. C. Gunawan, E. R. Choban, J. E. Conour, J. Silvestre, L. B. Schook, H. R. Gaskins, D. E. Leckband, P. J. A. Kenis, *Langmuir* **2005**, *21*, 3061.
[18] K. A. Fosser, R. G. Nuzzo, *Anal. Chem.* **2003**, *75*, 5775.
[19] I. Caelen, A. Bernard, D. Juncker, B. Michel, H. Heinzelmann, E. Delamarche, *Langmuir* **2000**, *16*, 9125.
[20] L. Song, S. M. Nadkarni, H. U. Bodeker, C. Beta, A. Bae, C. Franck, W. J. Rappel, W. F. Loomis, E. Bodenschatz, *Eur. J. Cell Biol.* **2006**, *85*, 981.
[21] J. R. Tse, A. J. Engler, *PLoS One* **2011**, *6*, e15978.
[22] E. D. Ker, A. S. Nain, L. E. Weiss, J. Wang, J. Suhan, C. H. Amon, P. G. Campbell, *Biomaterials* **2011**, *32*, 8097.
[23] J. A. Phillippi, E. Miller, L. Weiss, J. Huard, A. Waggoner, P. Campbell, *Stem Cells* **2008**, *26*, 127.
[24] J. He, Y. Du, Y. Guo, M. J. Hancock, B. Wang, H. Shin, J. Wu, D. Li, A. Khademhosseini, *Biotechnol. Bioeng.* **2011**, *108*, 175.
[25] Y. Du, M. J. Hancock, J. He, J. L. Villa-Uribe, B. Wang, D. M. Cropek, A. Khademhosseini, *Biomaterials* **2010**, *31*, 2686.
[26] S. Hong, S. J. Song, J. Y. Lee, H. Jang, J. Choi, K. Sun, Y. Park, *J. Biosci. Bioeng.* **2013**, *116*, 224.
[27] F. Xu, B. Sridharan, S. Wang, U. A. Gurkan, B. Syverud, U. Demirci, *Biomicrofluidics* **2011**, *5*, 22207.
[28] S. Tasoglu, U. Demirci, *Trends Biotechnol.* **2013**, *31*, 10.
[29] K. Jakab, C. Norotte, F. Marga, K. Murphy, G. Vunjak-Novakovic, G. Forgacs, *Biofabrication* **2010**, *2*, 022001.
[30] M. Gruene, M. Pflaum, A. Deiwick, L. Koch, S. Schlie, C. Unger, M. Wilhelmi, A. Haverich, B. N. Chichkov, *Biofabrication* **2011**, *3*, 015005.
[31] D. F. Duarte Campos, A. Blaeser, M. Weber, J. Jakel, S. Neuss, W. Jahnen-Dechent, H. Fischer, *Biofabrication* **2013**, *5*, 015003.
[32] S. Catros, J. C. Fricain, B. Guillotin, B. Pippenger, R. Bareille, M. Remy, E. Lebraud, B. Desbat, J. Amedee, F. Guillemot, *Biofabrication* **2011**, *3*, 025001.
[33] W. Saadi, S. W. Rhee, F. Lin, B. Vahidi, B. G. Chung, N. L. Jeon, *Biomed. Microdevices* **2007**, *9*, 627.
[34] Y. Shin, J. S. Jeon, S. Han, G.-S. Jung, S. Shin, S.-H. Lee, R. Sudo, R. D. Kamm, S. Chung, *Lab Chip* **2011**, *11*, 2175.
[35] B. Mosadegh, C. Huang, J. W. Park, H. S. Shin, B. G. Chung, S. K. Hwang, K. H. Lee, H. J. Kim, J. Brody, N. L. Jeon, *Langmuir* **2007**, *23*, 10910.
[36] S. Selimovic, W. Y. Sim, S. B. Kim, Y. H. Jang, W. G. Lee, M. Khabiry, H. Bae, S. Jambovane, J. W. Hong, A. Khademhosseini, *Anal. Chem.* **2011**, *83*, 2020.
[37] A. D. Stroock, G. J. McGraw, *Philos. Trans. A Math. Phys. Eng. Sci.* **2004**, *362*, 971.

[38] E. L. Baker, R. T. Bonnecaze, M. H. Zaman, *Biophys. J.* **2009**, *97*, 1013.
[39] P. A. Janmey, J. P. Winer, M. E. Murray, Q. Wen, *Cell Motil. Cytoskeleton* **2009**, *66*, 597.
[40] P. A. Janmey, J. P. Winer, J. W. Weisel, *J. R. Soc Interface* **2009**, *6*, 1.
[41] B. A. Aguado, W. Mulyasasmita, J. Su, K. J. Lampe, S. C. Heilshorn, *Tissue Eng. Part A* **2012**, *18*, 806.
[42] A. Ehninger, A. Trumpp, *J. Exp. Med. 208*, 421.
[43] M. Magnusson, H. K. Mikkola, *Cell Stem Cell* **2008**, *2*, 302.
[44] H. G. Kopp, S. T. Avecilla, A. T. Hooper, S. Rafii, *Physiology* **2005**, *20*, 349.
[45] J. Liao, K. E. Hammerick, G. A. Challen, M. A. Goodell, F. K. Kasper, A. G. Mikos, *J. Orthop. Res.* **2011**, *29*, 1544.
[46] C. Beta, T. Frohlich, H. U. Bodeker, E. Bodenschatz, *Lab Chip* **2008**, *8*, 1087.
[47] C. A. Klug, S. J. Morrison, M. Masek, K. Hahm, S. T. Smale, I. L. Weissman, *Proc. Natl. Acad. Sci. U.S.A.* **1998**, *95*, 657.
[48] S. Pedron, B. A. C. Harley, *J. Biomed. Mater. Res. A* **2013**, unpublished.
[49] K. Hosokawa, F. Arai, H. Yoshihara, H. Iwasaki, Y. Nakamura, Y. Gomei, T. Suda, *Blood* **2010**, *116*, 554.
[50] P. Kirstetter, K. Anderson, B. T. Porse, S. E. Jacobsen, C. Nerlov, *Nat. Immunol.* **2006**, *7*, 1048.
[51] T. D. Wheeler, D. Zeng, A. V. Desai, B. Onal, D. E. Reichert, P. J. Kenis, *Lab Chip* **2010**, *10*, 3387.
[52] B. A. Harley, H. D. Kim, M. H. Zaman, I. V. Yannas, D. A. Lauffenburger, L. J. Gibson, *Biophys. J.* **2008**, *95*, 4013.
[53] G. A. Challen, N. Boles, K. K. Lin, M. A. Goodell, *Cytometry A* **2009**, *75*, 14.
[54] L. Yang, D. Bryder, J. Adolfsson, J. Nygren, R. Mansson, M. Sigvardsson, S. E. Jacobsen, *Blood* **2005**, *105*, 2717.
[55] S. Okada, H. Nakauchi, K. Nagayoshi, S. Nishikawa, Y. Miura, T. Suda, *Blood* **1992**, *80*, 3044.
[56] Y. L. Yang, L. J. Kaufman, *Biophys. J.* **2009**, *96*, 1566.
[57] Y. Le, B. M. Zhu, B. Harley, S. Y. Park, T. Kobayashi, J. P. Manis, H. R. Luo, A. Yoshimura, L. Hennighausen, L. E. Silberstein, *Immunity* **2007**, *27*, 811.
[58] B. L. Sprague, R. L. Pego, D. A. Stavreva, J. G. McNally, *Biophys. J.* **2004**, *86*, 3473.
[59] B. L. Sprague, J. G. McNally, *Trends Cell Biol.* **2005**, *15*, 84.
[60] E. A. Reits, J. J. Neefjes, *Nat. Cell. Biol.* **2001**, *3*, E145.
[61] J. Lippincott-Schwartz, E. Snapp, A. Kenworthy, *Nat. Rev. Mol. Cell Biol.* **2001**, *2*, 444.
[62] R. K. Jain, R. J. Stock, S. R. Chary, M. Rueter, *Microvasc. Res.* **1990**, *39*, 77.
[63] R. M. Klein, A. E. Aplin, *Cancer Res.* **2009**, *69*, 2224.
[64] R. R. Sokal, *Cc/Agr Biol. Environ.* **1982**, 22.